Journal of Instrumentation

Development of advanced Thomson spectrometers for nuclear fusion experiments initiated by laser

Published by IOP Publishing for Sissa Medialab

Received: *June 15, 2020*
Accepted: *July 20, 2020*
Published: *October 8, 2020*

Plasma Physics by Laser and Applications (PPLA 2019)
Physics Department, University of Pisa, Pisa, Italy
29–31 October, 2019

Development of advanced Thomson spectrometers for nuclear fusion experiments initiated by laser

G. Di Giorgio,[a] **F. Consoli,**[a] **R. De Angelis,**[a] **P. Andreoli,**[a] **M. Cipriani,**[a,1] **G. Cristofari,**[a] **A. Bonasera,**[b,c] **M. Salvadori**[a,d,e] **and J. Sura**[f]

[a] *ENEA — C.R. Frascati, Fusion and Nuclear Safety Department, Frascati, Italy*
[b] *INFN-LNS, Catania, Italy*
[c] *Cyclotron Institute, Texas A&M University, College Station, Texas, U.S.A.*
[d] *Università di Roma La Sapienza, Rome, Italy*
[e] *INRS-EMT, Varennes, Québec, Canada*
[f] *Heavy Ions Laboratory, University of Warsaw, Warszawa, Poland*

E-mail: mattia.cipriani@enea.it

Abstract: Thomson Spectrometers are devices capable to separate the several particle species (with distinct charge-to-mass ratio and energy) produced by the different regimes of laser-matter experiments. In this work we describe the development of advanced spectrometers for low and medium energy particles. In particular, they are suitable for protons in the 5 keV–2 MeV and 100 keV–10 MeV energy ranges, respectively. The new prototypes of spectrometers have been designed and built to have a high sensitivity and be adaptable to many experimental situations and configurations, and are tailored to the characterization of charged particles and products of nuclear fusion reactions initiated by high energy and intensity lasers. Details on the realized prototypes, on their characterization and testing, together with the first experimental results are discussed.

Keywords: Plasma diagnostics - charged-particle spectroscopy; Spectrometers; Erasable phosphors; Plasma generation (laser-produced, RF, x ray-produced)

[1] Corresponding author.

https://doi.org/10.1088/1748-0221/15/10/C10013

2020 JINST 15 C10013

Contents

2020 JINST 15 C10013

1 Introduction

Laser-plasma interaction generates charged and neutral particles, along with electromagnetic waves, with frequencies ranging from RF-microwaves to gamma rays [1]. The detection of charged particles is of fundamental importance in laser-matter experiments. It provides information about the physical aspects of the interaction, such as parametric instabilities, particle acceleration and, in the context of inertial confinement fusion, fusion reactions. Various techniques can be employed in diagnosing particles from laser-plasma interaction, such as Time Of Flight (TOF), track detectors (CR39, PM355,. . .), scintillators, electrostatic and magnetostatic spectrometers [1–3]. TOF detectors provide information about the particle velocity, but do not discriminate between the various species. The particle spectrum can be calculated from TOF data, but only supposing the particle species on the basis of physical considerations [4–6]. Similarly, magnetic spectrometers relate the particle properties with the deflection, but they are useful only when the particle species is known, for example with electron beams. Track detectors can provide the number of particles and also can give some kind of discrimination between the various species, when suitable filters are used [7–9]. In laser-plasma interaction experiments, multiple particle species are generated, such as electrons, protons, and ions. In some cases, charged molecules may be produced, too. Thomson spectrometers are very useful in discriminating the particle species in this context, with also measuring their energy spectrum. This is achieved by deflecting particles coming from a pinhole by both electric and magnetic fields and making them impinge on a detector, where they draw 2D curves (parabolas) defined by their charge-to-mass ratio [10–12].

In general the electrostatic and magnetostatic deflection are done in two different stages and the spectrometers are quite long structures [13–15] and for this reason in common experiments they often find place in extensions of the vacuum flanges, so at rather long distance from target. To maximize the signal-to-noise ratio on the detector and in general to increase the sensitivity of the detection method, the spectrometer should be located as close to the interaction point as possible. However, this strategy poses some limits on the measurements. First, the intense X-ray flux produced by laser-target interaction can cause, without proper shielding, a strong background noise on typical detectors such as Imaging Plates (IPs), which lowers the sensitivity of the spectrometer. Second, the strong Electromagnetic Pulses (EMPs) in the radio-frequency microwave regime generated during the interaction [16] could alter the deflecting fields, leading to modulation of the expected traces and possible superimposition of them, with loss of reliability on particle discrimination. Both these two considered effects increase their intensity when getting closer to the target, and then become of primary importance whenever the spectrometers are intended to be placed rather close to the interaction point. Lastly, mounting a large structure inside the vacuum chamber and close to the target is not always a simple task, because of the multiple objects already present in many experimental setups.

The purpose of this work is the description of two specific Thomson spectrometers tailored to the analysis of experiments of fusion reactions triggered by laser-matter interaction. The main focus has been given to the enhancement of the sensitivity and of the robustness to background, due either to EMP or to ionizing radiation. Advanced technological solutions were found and optimized in this sense. We based these new spectrometers on the studies and developments already discussed in reference [12]. In particular, we improved the design of the deflecting structure for two different energy ranges, realizing two prototypes named “SMALL” and “BIG”. The SMALL spectrometer is suitable for protons with energies in the range 5 keV - 2 MeV, whereas the BIG spectrometer for those with energies from 100 keV to 10 MeV. The first spectrometer was meant for having a detailed description of the plasma parameters of the interaction, whereas the BIG was optimized also for the detection of fusion products. The high sensitivity of these devices and their optimization for being placed quite close to the interaction point, make them suitable candidates for the accurate characterizations of ions produced in experiments of low-rate fusion reactions triggered by laser [12, 17]. For each of them, a suitable compact casing has been designed, with the focus on the increase of the signal-to-noise ratio on the detector. Two types of passive detectors are foreseen: Imaging Plates for a fast and easy readout of the obtained traces, but which suffer of limited sensitivity, and then CR39 track detectors, well known for the remarkable sensitivity, but also for the slow and complex measurement analysis. Electrical contacts for powering the electrodes were placed on a side of the casing with suitable shielding against EMPs.

2 Operating principle and modeling

The basic scheme of the Thomson spectrometers is shown in figure 1. The ions emitted from the target as a result of the laser-matter interaction pass through a double-pinhole structure, are deflected by the magnetic and electric fields and then intercept the detector. The tracks left on it have the shape of parabolas. As will be discussed in subsection 3.1, the electrode assembly is very compact, which implies that the electrodes are very short. In this situation, the fields outside of the assembly play an important role and have to be considered in modeling the behavior of the ions in the spectrometer.

2020 JINST 15 C10013

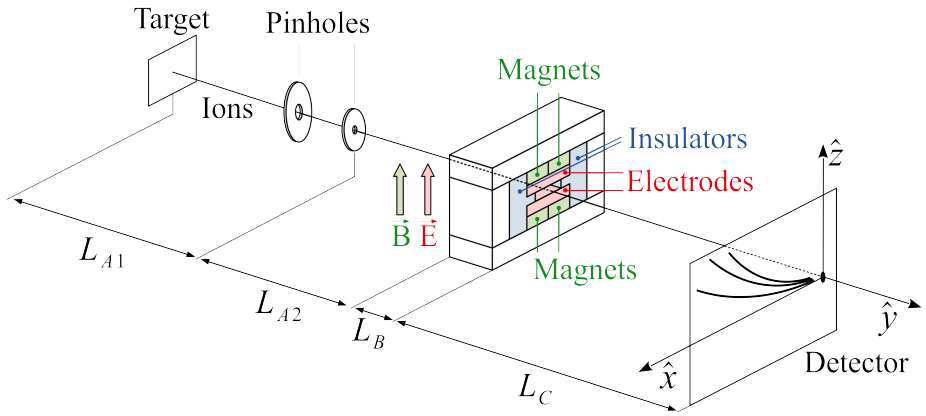

Figure 1. Operating scheme of the Thomson spectrometers.

In reference [12] useful approximate relations were derived for ions at energies such that the related curvature radius in the spectrometer is much higher than the spectrometer length. According to them, the coordinates of interception of the ions on the detector (see figure 1) are obtained as

$$x = \frac{q_i}{\sqrt{2m_i E_i}} A_B \,, \tag{2.1}$$

$$z = \frac{q_i}{2E_i} A_E \,, \tag{2.2}$$

where q_i is the charge, m_i the mass and E_i is the energy of the incident ion. A_B and A_E are integrals of the electric and magnetic fields along the propagation direction of the particles

$$A_B = \int_0^{L_{A1}+L_{A2}+L_B+L_C} \int_0^y B_\perp(\zeta)\, d\zeta\, dy \,, \tag{2.3}$$

$$A_E = \int_0^{L_{A1}+L_{A2}+L_B+L_C} \int_0^y E_\perp(\zeta)\, d\zeta\, dy \,. \tag{2.4}$$

Eliminating E_i the equation for the parabola is

$$z = \frac{m_i A_E}{q_i A_B^2} x^2 \,, \tag{2.5}$$

which passes from the axes origin and depends on the q_i/m_i ratio, allowing for the discrimination of the ion species.

Sensitivity is of primary importance for the detection of fusion products in these low-rate reactions. The actual solid angle covered and the target-pinhole distance determine the detection capability of the device. According to the scheme of figure 1, under the hypothesis of point emission of particles from the laser-matter interaction site, the size of the traces is

$$S_t \simeq 2\,(L_{A1} + L_{A2} + L_B + L_C)\,\sqrt{\Omega/\pi} \tag{2.6}$$

being $\Omega = (\pi/4)(\varphi_p/L_{A1})^2$ the solid angle of detection and φ_p the pinhole diameter. The constraint on the maximum acceptable S_t is related to the maximum values of the electric and magnetic fields. This sets a limitation for the covered solid angle, and thus for the sensitivity. But the intense fields,

2020 JINST 15 C10013

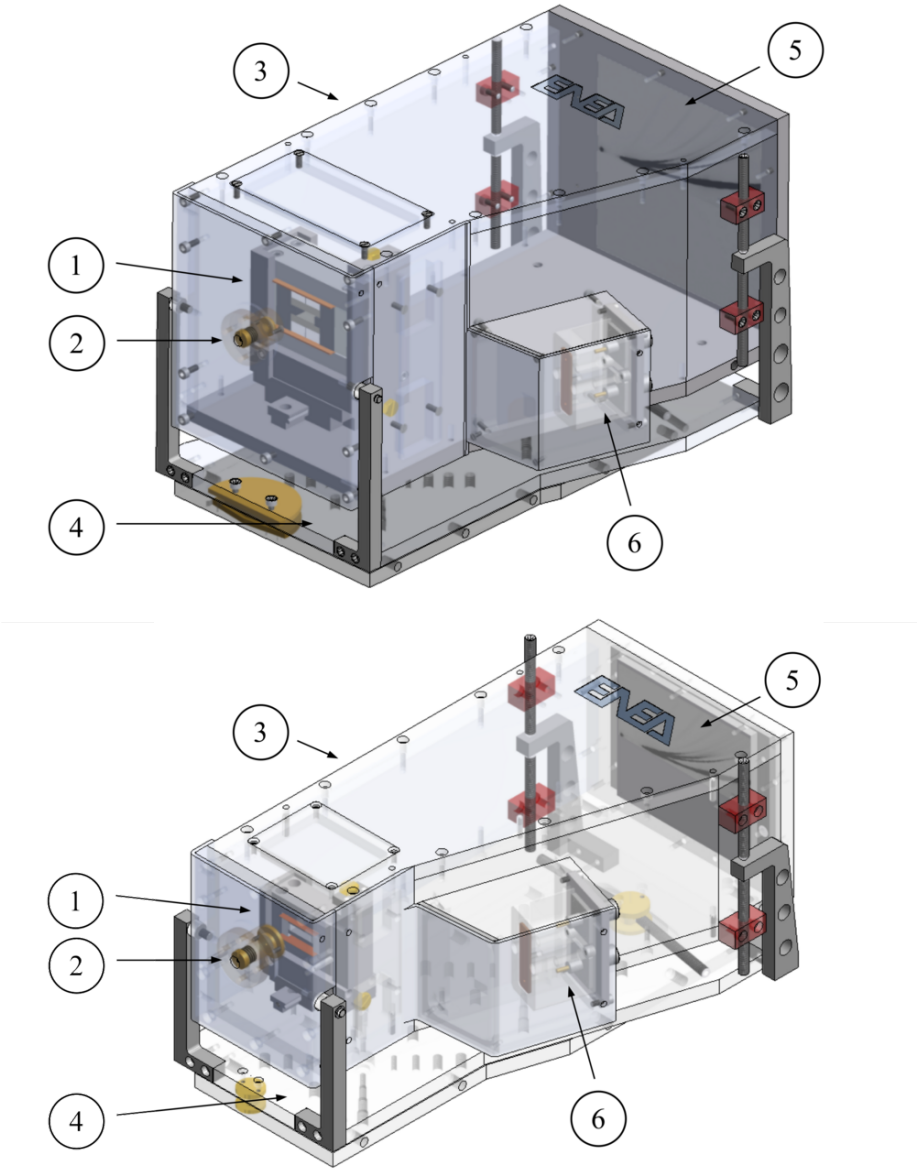

Figure 2. Technical drawing of the BIG (upper) and SMALL (lower) spectrometer devices. The numbers refer to the single parts, as indicated in the text.

needed to have good trace separation, usually implies large dimensions of the device, and this can be an issue for the spectrometer when positioned close to the target, so for low L_{A1}. A compromise was here obtained on the purpose to optimize the sensitivity.

3 The spectrometers

The spectrometers described in this work are presented in figure 2. Both spectrometers are constituted by the same principle components and their dimensions change according to the design needs. The parts of the devices, as indicated in figure 2 are:

2020 JINST 15 C10013

1. The deflecting-field assembly.
2. The two-pinhole assembly.
3. The external casing.
4. The tilt-and-yaw adjustments support.
5. The detector and alignment laser supports.
6. The high voltage connectors.

The following subsections contain a description of each component.

3.1 The deflecting-field assembly

The design of the deflecting-field assemblies is similar to that described in ref. [12]. As mentioned in the Introduction, two different structures have been realized, in order to cover two different energy ranges. The SMALL spectrometer is designed to detect ions with energies from 5 keV to 2 MeV; the BIG spectrometer is for ion energy in the range 100 keV–10 MeV. Figure 3 shows the schematics of the two deflecting structures, which have the same layout but different dimensions.

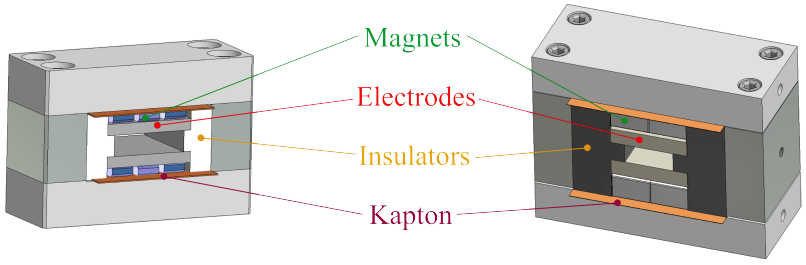

Figure 3. The design of the SMALL (left) and BIG (right) deflecting field assembly, with the identification of the various components.

Table 1. Overall operating parameters of the SMALL and BIG spectrometers.

	SMALL	BIG
Maximum measured voltage	±3.2 kV	±3.9 kV
Electrode length	16 mm	25 mm
Electrode gap	4 mm	5 mm
Maximum derived electric field	1.6 MV/m	1.56 MV/m
Maximum measured magnetic field	2.2 kG	4.0 kG

To avoid contamination of the deflecting fields from the EMPs generated during the laser-target interaction, permanent Neodymium magnets are used in the spectrometers. This also allows for easy scalability of the magnetic field. The short electrode length allows for reduced effects of possible EMP fields on particle deflection, especially for fast ions. The spectrometers have simultaneous magnetostatic and electrostatic deflection, with the magnets and electrodes having the

2020 JINST 15 C10013

same length and width and being kept in place by a robust soft iron structure, which counterbalance the repulsive magnetic forces. Kapton foils are placed between the electrodes and the iron structure for insulation, avoiding electrical discharges. The magnets-electrodes assembly is further stabilized and isolated by Teflon and Ertalon elements, indicated in figure 1 as "Insulators". The overall operating parameters of the two spectrometers are reported in table 1.

3.2 The two-pinhole assembly

A noticeable contribution to the background noise due to X-rays on the IP may come from the bremsstrahlung X-rays produced by the interaction of electrons entering the detector with the walls of the casing. In fact, being much lighter than protons, electrons are deflected on a very short distance as they enter the spectrometer. Therefore, as shown in the diagram of figure 4, the use of two pinholes at the casing entrance allows the collection of low energy electrons in the cavity between them. In this way, the residual X-ray background is lowered and the signal-to-noise ratio on the detector is increased. Drawings of the two-pinholes assemblies are reported in figure 4. Table 2 contains the specifications of the two-pinholes assembly for the SMALL and the BIG spectrometers.

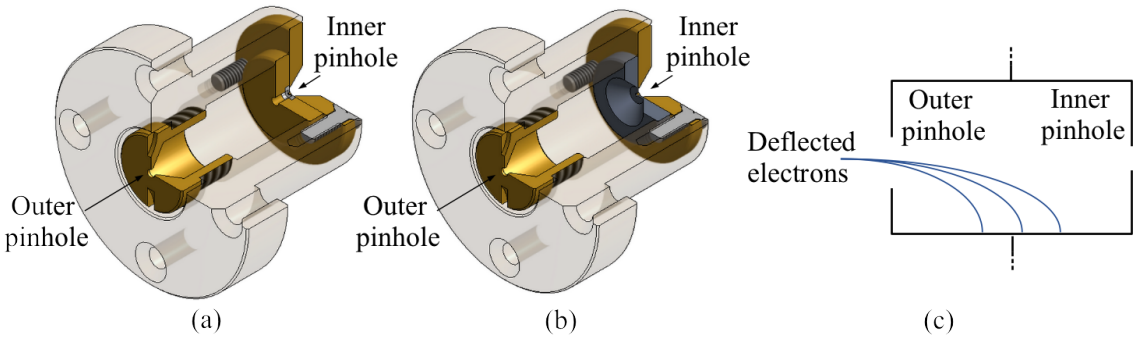

Figure 4. (a,b) Technical drawings of the two-pinholes assembly for the SMALL (a) and BIG (b) spectrometer; (c) the scheme of the structure.

Table 2. Specifications of the two-pinholes assembly for the SMALL and BIG spectrometers.

	SMALL		BIG	
Pinhole	Outer	Inner	Outer	Inner
Material	Brass	Pt-Ir	Brass	Pb
Diameter (mm)	1.0	0.2	2.0	0.35
Minimum pinhole thickness (mm)		0.1		0.2

3.3 The external casing

The compactness of these spectrometer configurations allows to easily place them inside most of the experimental chambers, at close proximity of the target. This implies that the spectrometers would be facing intense fluxes of X-rays, coming from the bremsstrahlung of the particles in the laser-produced plasma and from the interaction of the accelerated particles with the walls of the experimental chamber and with the other objects inside it. This may cause strong noise on the

2020 JINST 15 C10013

detector. On the front of the casing, lead screens provide efficient shielding against this radiation and reduce the background noise on the detector. According to the specific experiment where the spectrometer will be used, better protection can be added externally, on necessity. In addition, strong EMPs are known to be generated by the laser-matter interaction, up to some MV/m or more, which could affect the reliability of the detector. The spectrometers are therefore inserted in an aluminum casing, which has been designed for shielding efficiently the EMPs and to provide a reliable support for the positioning of the spectrometer in any experimental setup. Drawings of the casings for the SMALL and BIG spectrometers are shown in figure 5, along with the dimensions, reported in table 3. As can be seen from the picture, on the left and right sides of the casings, a mechanism with four screws (red blocks) allows for fine control of the tilt and the yaw of the spectrometer by using the yaw and tilt support described in subsection 3.4.

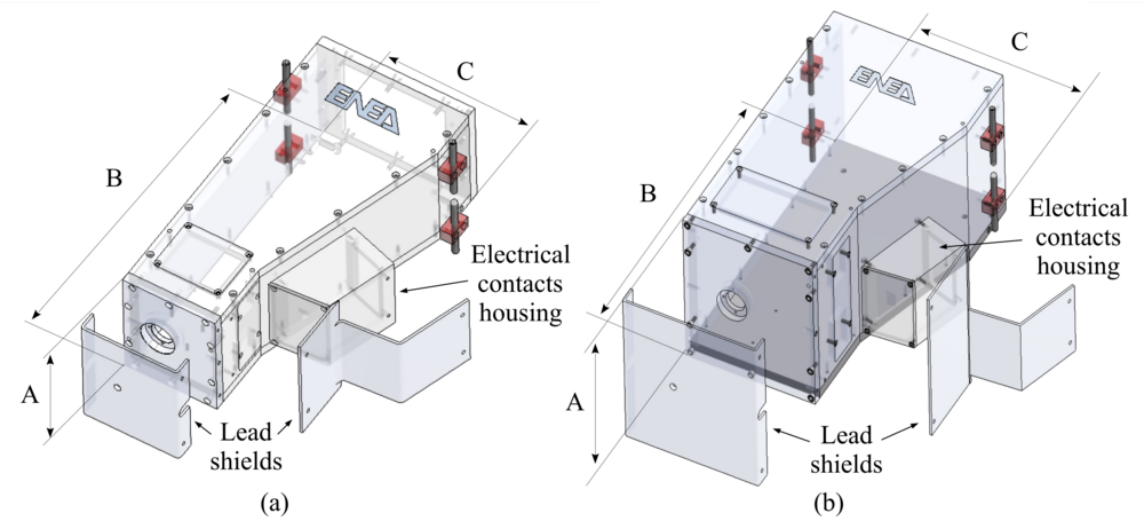

Figure 5. Drawings of the casings for the SMALL (left) and BIG (right) Thomson spectrometers. Lead shields are visible on the front and the right side of each casing. The hole on the front of the casings houses the two-pinhole assemblies. The small opening on the upper part of each casing gives direct access to the deflecting field assembly without completely opening the top cover. On the right of each casing the housing for the electrical contacts is visible.

Table 3. Dimensions of the casings of the spectrometers, as indicated in figure 5.

	SMALL	BIG
A (mm)	92	131
B (mm)	262	275
C (mm)	158	201

3.4 Tilt and yaw adjustment support

The support shown in figure 6 is placed on the bottom of the casing of each spectrometer. Thanks to this component, the spectrometer can be easily placed in the experimental chamber and can be precisely aligned with the point of interaction of the laser on the target, to maximize the particle yield.

2020 JINST 15 C10013

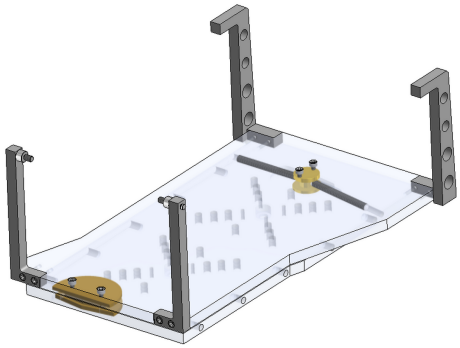

Figure 6. The yaw and tilt adjustments support for the BIG spectrometer. For the SMALL spectrometer the design is similar.

3.5 The detector and alignment support

The charged particles enter the spectrometer from the two-pinholes assembly, are deflected by the magnetostatic and electrostatic fields and reach the plate on the rear side of the spectrometer. IP and CR-39 detectors can be mounted on the plate by using suitable holders, shown in figure 7. A different plate, holding a visible laser diode (rightmost picture in figure 7), can be installed in place of the detector plate in order to align the spectrometer with the target during the preparation of the experimental setup. The laser beam is first aligned with the two pinholes on the front of the spectrometer by using the movements of the laser holder. Then, by using the adjustment plate described in subsection 3.4, the spectrometer line of sight can be set precisely on the target.

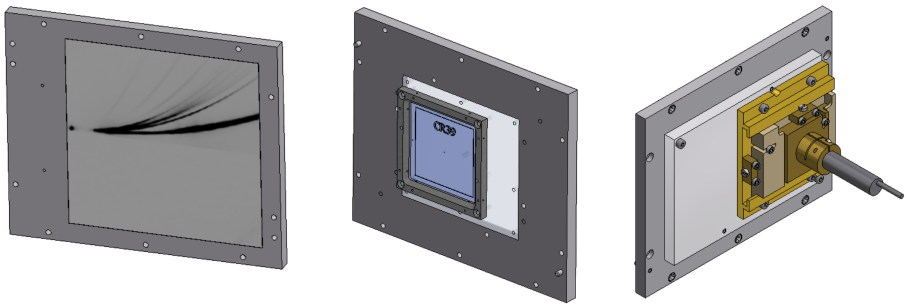

Figure 7. The various supports for the IP (left), the CR-39 (middle) and the support for the alignment laser (right). For brevity, the plates in this picture are relative to the BIG spectrometer. The ones of the SMALL spectrometer are analogous.

3.6 High-voltage connectors

The high-voltage connectors, identified with “VOLT UP” and “VOLT DOWN”, for powering the electrodes of the deflecting field assembly are placed on the right side of the casing of each spectrometer. Proper shielding against EMPs allows for reliable operation even in harsh environments, where intense electromagnetic fields are generated by the laser-matter interaction. The spectrometer is equipped with double-shielded RG223/U cables to further avoid background from EMPs. A

2020 JINST 15 C10013

drawing of the high-voltage MHV connectors is shown in figure 8 and is practically identical for both the SMALL and the BIG spectrometers.

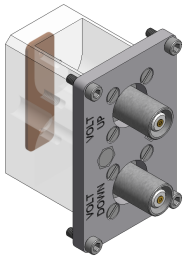

Figure 8. The high-voltage connectors for the spectrometers. The same design has been used for both the SMALL and BIG spectrometers.

4 Experimental results

The two spectrometers have been preliminary tested at the ABC laser facility, at the ENEA Research Center in Frascati. The ABC laser is a Nd:phosphate glass laser which can deliver two counter-propagating beams with 100 J of energy each at the fundamental wavelength $\lambda_L = 1054$ nm. The temporal duration of the pulses is of 3 ns Full Width Half Maximum and the maximum intensity on the target is about 10^{15} W/cm^2.

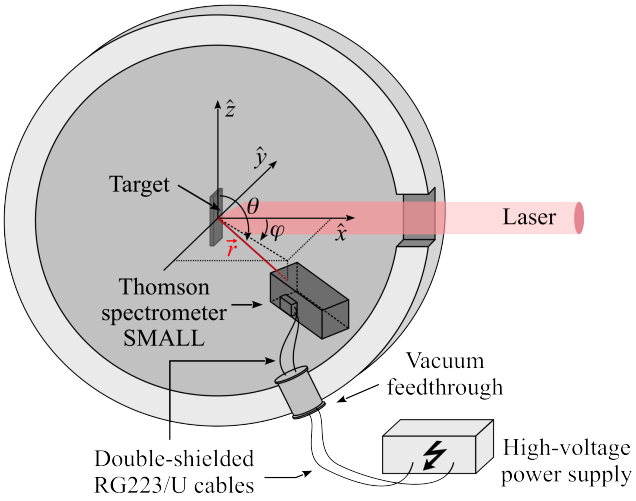

Figure 9. The setup of the experiments. The spectrometer was aligned with the interaction point and the position of the external pinhole had the coordinates $|\vec{r}| = 254$ mm, $\theta = 108°$ and $\varphi = -50°$.

The experimental setup used is reported in figure 9. The results shown in this work are relative to the SMALL spectrometer, which was placed inside the experimental chamber at coordinates $|\vec{r}| = 254$ mm, $\theta = 108°$ and $\varphi = -50°$ and aligned with the interaction point. Imaging plates Fujifilm BAS-TR2040 were used as detectors in the experiments and were read by using the Durr CR 35 BIO scanner [18]. Figure 10 shows the results of the shot #5804. The target was a polystyrene

2020 JINST 15 C10013

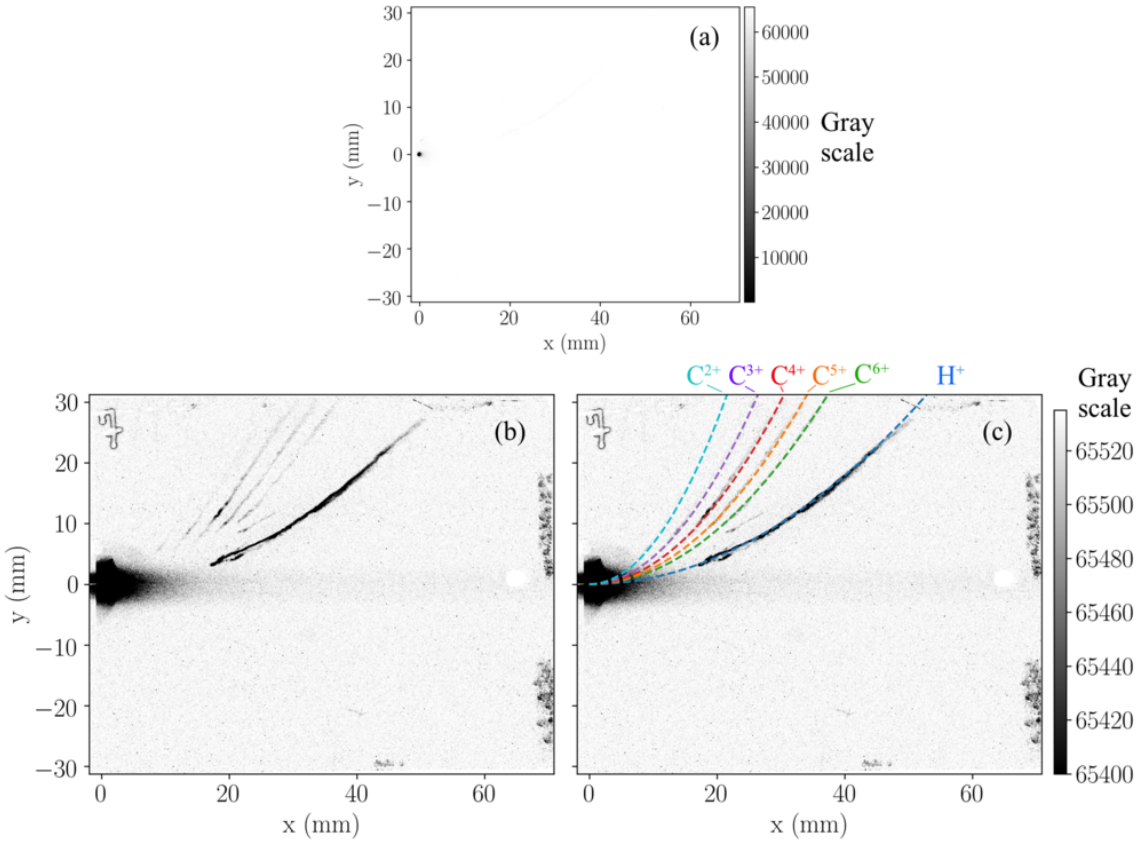

Figure 10. The results of the analysis of the IP for the shot #5804. (a) The original image as read by the Durr scanner. The black area at the axes origin is the track left by the X-rays which passed through the pinholes. (b) The same image with an increased contrast to make the tracks of the ions more visible. (c) The same as (b) with the superimposition of the calculated curves.

foam with an average density of 10 mg/cm^3, an average pore size of 50 μm and a thickness of 520 µm. The laser energy was $E = 37.7$ J for an intensity on the target $I \simeq 10^{14}$ W/cm^2.

Figure 10a shows the original reading of the Durr scanner. The black area at the axes origin is the track left by the X-rays which passed through the pinholes. This track can be used as a reference for the intersection of the direction of the line of sight of the spectrometer with the detector, setting the origin of the curves made by the ions. Increasing the contrast reveals the tracks left by the particles on the IP, as shown in figure 10b. From these tracks, the fitting curves can be calculated by using the laws (2.1-2.2) and the various ion species can be identified. The result of this procedure is reported for the shot #5804 in figure 10c. From the analysis, the proton energy range has been found to be 8.5 keV–75 keV and clear signature of the different charge states of Carbon were obtained, as well.

5 Conclusions

In this work two new compact Thomson spectrometers have been described. A SMALL and a BIG configurations have been designed and constructed to reveal and discriminate ions with energies in the ranges 5 keV–2 MeV and 100 keV–10 MeV, respectively. All the components have been

2020 JINST 15 C10013

discussed in detail. The design of the spectrometers is conceived to reduce the background noise on the detector by means of an appropriate shielding against X-rays. Moreover, the design allows to avoid the perturbation of the electric fields due to the coupling of the EMPs generated by the laser-matter interaction with the cables from the power supply. The spectrometers are built for an easy and quick mounting and include a built-in alignment device for faster setup and reliable operation in the experiments. The compactness of the spectrometers makes them very suitable to be used in cluttered experimental chambers, even when very little space is available. The possibility to place these devices rather close to the interaction point and their intrinsic sensitivity even in the harsh conditions that this proximity induces, make them suitable candidates for the accurate characterizations of ions produced in experiments of low-rate fusion reactions triggered by laser [12, 17]). The first tests performed on them in experiments at the ABC laser facilty showed their correct operation even at low distances from the target. In these experimental conditions and positions EMP values of several tens of kV/m were sensed [19–22] but, as observed in figure 10, no modulation of the parabolic traces, instead expected in cases with intense EMP levels, was observed. This is a good experimental confirmation of the robust design and operation of the devices.

Acknowledgments

This work has been carried out within the framework of the EUROfusion Enabling Research Project and has received funding from the Euratom research and training programme 2014–2018 and 2019–2020 under grant agreement No 633053. The views and opinions expressed herein do not necessarily reflect those of the European Commission. F. Consoli acknowledges fruitful discussions with M. Scisciò from ENEA.

References

[1] W. Kruer, *The Physics of Laser Plasma Interactions*, Frontiers in Physics, Avalon Publishing (2003).

[2] G. Münzenberg, *Development of mass spectrometers from Thomson and Aston to present*, *Int. J. Mass Spectrom.* **349–350** (2013) 9.

[3] P. Bolton, M. Borghesi, C. Brenner, D. Carroll, C. De Martinis, F. Fiorini et al., *Instrumentation for diagnostics and control of laser-accelerated proton (ion) beams*, *Phys. Med.* **30** (2014) 255.

[4] M. Cipriani, F. Consoli, P. Andreoli, D. Batani, A. Bonasera, G. Boutoux et al., *Spectral characterization by CVD diamond detectors of energetic protons from high-repetition rate laser for aneutronic nuclear fusion experiments*, 2009 *JINST* **14** C01027.

[5] M. Salvadori, F. Consoli, C. Verona, M. Cipriani, M. Anania, P. Andreoli et al., *Accurate spectra for high energy ions by advanced time-of-flight diamond-detector schemes in experiments with high energy and intensity lasers*, submitted to *Sci. Rep.* (2020) arXiv:2003.01442.

[6] C. Verona, M. Marinelli, S. Palomba, G. Verona-Rinati, M. Salvadori, M. Cipriani et al., *Comparison of single crystal diamond TOF detectors in planar and transverse configuration*, 2020 *JINST* **15** C09066.

[7] S.A. Durrani and R.K. Bull, *Solid State Nuclear Track Detection: Principles, Methods, and Applications*, International Series in Natural Philosophy, vol. 111, Pergamon Press, Oxford/New York (1987).

2020 JINST 15 C10013

[8] D. Nikezic and K. Yu, *Formation and growth of tracks in nuclear track materials*, *Mat. Sci. Eng. R* **46** (2004) 51.

[9] T.W. Jeong, P. K. Singh, C. Scullion, H. Ahmed, P. Hadjisolomou, C. Jeon et al., *CR-39 track detector for multi-MeV ion spectroscopy*, *Sci. Rep.* **7** (2017) 2152.

[10] J.J. Thomson, *Rays of positive electricity*, *Proc. Royal Soc. Lond. A* **89** (1913) 1.

[11] J.N. Olsen, G.W. Kuswa and E.D. Jones, *Ion-expansion energy spectra correlated to laser plasma parameters*, *J. Appl. Phys.* **44** (1973) 2275.

[12] F. Consoli, R. De Angelis, A. Bonasera, J. Sura, P. Andreoli, G. Cristofari et al., *Study on a compact and adaptable Thomson Spectrometer for laser-initiated* $^{11}B(p,\alpha)^{8}Be$ *reactions and low-medium energy particle detection*, 2016 *JINST* **11** C05010.

[13] D. Carroll, P. Brummitt, D. Neely, F. Lindau, O. Lundh, C.-G. Wahlström et al., *A modified Thomson parabola spectrometer for high resolution multi-MeV ion measurements—Application to laser-driven ion acceleration*, *Nucl. Instrum. Meth. A* **620** (2010) 23.

[14] D. Jung, R. Hörlein, D. Kiefer, S. Letzring, D.C. Gautier, U. Schramm et al., *Development of a high resolution and high dispersion Thomson parabola*, *Rev. Sci. Instrum.* **82** (2011) 013306.

[15] J.A. Cobble, K.A. Flippo, D.T. Offermann, F.E. Lopez, J.A. Oertel, D. Mastrosimone et al., *High-resolution Thomson parabola for ion analysis*, *Rev. Sci. Instrum.* **82** (2011) 113504.

[16] F. Consoli, V.T. Tikhonchuk, M. Bardon, P. Bradford, D.C. Carroll, J. Cikhardt et al., *Laser produced electromagnetic pulses: Generation, detection and mitigation*, *High Power Laser Sci. Eng.* **8** (2020) e22.

[17] F. Consoli, R. De Angelis, P. Andreoli, A. Bonasera, M. Cipriani, G. Cristofari et al., *Methodologies of diagnostics for products of laser-initiated* $^{11}B(p,\alpha)^{2}\alpha$ *fusion reactions*, accepted in *Front. Phys.* (2020).

[18] F. Ingenito, P. Andreoli, D. Batani, G. Boutoux, M. Cipriani, F. Consoli et al., *Comparative calibration of IP scanning equipment*, 2016 *JINST* **11** C05012.

[19] F. Consoli, R. De Angelis, L. Duvillaret, P.L. Andreoli, M. Cipriani, G. Cristofari et al., *Time-resolved absolute measurements by electro-optic effect of giant electromagnetic pulses due to laser-plasma interaction in nanosecond regime*, *Sci. Rep.* **6** (2016) 27889.

[20] F. Consoli, R. De Angelis, P. Andreoli, M. Cipriani, G. Cristofari, G. Di Giorgio et al., *Experiments on Electromagnetic Pulse (EMP) generated by laser-plasma interaction in nanosecond regime*, in proceedings of the 15^{th} *International Conference on Environment and Electrical Engineering (EEEIC)*, Rome, Italy, 10–13 June 2015, pp. 182–187.

[21] F. Consoli, R. De Angelis, P. Andreoli, G. Cristofari and G. Di Giorgio, *Measurement of the Radiofrequency-microwave Pulse Produced in Experiments of Laser-plasma Interaction in the ABC Laser Facility*, *Phys. Procedia* **62** (2015) 11.

[22] F. Consoli, R. De Angelis, P. Andreoli, G. Cristofari, G. Di Giorgio, A. Bonasera et al., *Diagnostics improvement in the ABC facility and preliminary tests on laser interaction with light-atom clusters and* $p+^{11}B$ *targets*, *Nucl. Instrum. Meth. A* **720** (2013) 149.

2020 JINST 15 C10013